In Vivo Measurements of Cortical Thickness and Porosity at the Proximal Third of the Tibia Using Guided Waves: Comparison with Site-Matched Peripheral Quantitative Computed Tomography and Distal High-Resolution Peripheral Quantitative Computed Tomography

Johannes Schneider, Donatien Ramiandrisoa, Gabriele Armbrecht, Zully Ritter, Dieter Felsenberg, Kay Raum, Jean-Gabriel Minonzio

Ultrasound in Med. & Biol., Vol. 45, No. 5, pp. 1234–1242, 2019

0301-5629/$ - see front matter

https://doi.org/10.1016/j.ultrasmedbio.2019.01.008

● *Original Contribution*

IN VIVO MEASUREMENTS OF CORTICAL THICKNESS AND POROSITY AT THE PROXIMAL THIRD OF THE TIBIA USING GUIDED WAVES: COMPARISON WITH SITE-MATCHED PERIPHERAL QUANTITATIVE COMPUTED TOMOGRAPHY AND DISTAL HIGH-RESOLUTION PERIPHERAL QUANTITATIVE COMPUTED TOMOGRAPHY

JOHANNES SCHNEIDER,* DONATIEN RAMIANDRISOA,†,‡ GABRIELE ARMBRECHT,§ ZULLY RITTER,§ DIETER FELSENBERG,§ KAY RAUM,* and JEAN-GABRIEL MINONZIO†,¶

* Berlin-Brandenburg School for Regenerative Therapies (BSRT), Charité–Universitätsmedizin Berlin, Berlin, Germany; † Laboratoire d'Imagerie Biomédicale (LIB), Sorbonne University, CNRS, INSERM, Paris, France; ‡ BleuSolid, Pomponne, France; § Center for Muscle and Bone Research (ZMK), Charité–Universitätsmedizin Berlin, Berlin, Germany; and ¶ Escuela de Ingeniería Civil en Informática, Universidad de Valparaíso, Valparaíso, Chile

(*Received* 21 *September* 2018; *revised* 20 *December* 2018; *in final from* 8 *January* 2019)

Abstract—The aim of this study was to estimate cortical porosity (Ct.Po) and cortical thickness (Ct.Th) using 500-kHz bi-directional axial transmission (AT). $Ct.Th_{AT}$ and $Ct.Po_{AT}$ were obtained at the tibia in 15 patients from a 2-D transverse isotropic free plate model fitted to measured guided wave dispersion curves. The velocities of the first arriving signal (υ_{FAS}) and A_0 mode (υ_{A0}) were also determined. Site-matched peripheral quantitative computed tomography (pQCT) provided volumetric cortical bone mineral density ($Ct.vBMD_{pQCT}$) and $Ct.Th_{pQCT}$. Good agreement was found between $Ct.Th_{AT}$ and $Ct.Th_{pQCT}$ ($R^2 = 0.62$, root mean square error [RMSE] = 0.39 mm). $Ct.vBMD_{pQCT}$ correlated with $Ct.Po_{AT}$ ($R^2 = 0.57$), υ_{FAS} ($R^2 = 0.43$) and υ_{A0} ($R^2 = 0.28$). Furthermore, a significant correlation was found between AT and distal high-resolution pQCT. The measurement of cortical parameters at the tibia using guided waves might improve the prediction of bone fractures in a cost-effective and radiation-free manner. (E-mail: kay.raum@charite.de)

Key Words: **Axial transmission ultrasound, Cortical bone porosity, Guided waves, Peripheral quantitative computed tomography, Dual-energy X-ray absorptiometry.**

INTRODUCTION

The diagnosis of osteoporosis is currently based on areal bone mineral density (aBMD) measured by dual-energy X-ray absorptiometry (DXA), the current gold standard technique. However, a majority of bone fractures occur in patients who are not classified osteoporotic according to the current aBMD criteria (T-score < -2.5) (Schuit et al. 2004; Wainwright et al. 2005). This might be due to the technique's limited capacity to capture bone microstructure and differentiate between trabecular and cortical compartments. High-resolution peripheral quantitative computed tomography (HR-pQCT) is an advanced *in vivo* imaging technology that provides 3-D characterization of trabecular and cortical bone at the distal radius and tibia (Boyd 2008). Recent clinical studies using HR-pQCT have reported that bone microstructure and volumetric bone mineral density (vBMD) are associated with genetic disorder (Neto et al. 2017), effect of treatment (Lespessailles et al. 2016) and fracture (Sundh et al. 2017). However, HR-pQCT cannot easily be used for population-based screening because it is expensive, voluminous, non-portable and based on ionizing radiation. Cost-effective and radiation-free systems for the measurement of bone microstructure are needed to improve the prevention of fragility fractures in our society.

Ultrasound-based solutions are attractive because they are low cost, portable and non-ionizing. The heel (calcaneus) scanner was among the first devices using the transverse transmission configuration (emitter and receiver placed on opposite sites) to measure ultrasound

Address correspondence to: Kay Raum, Berlin-Brandenburg School for Regenerative Therapies, Charité–Universitätsmedizin Berlin, Augustenburger Platz 1, 13353 Berlin, Germany. E-mail: kay.raum@charite.de

propagation through trabecular bone (Langton and Njeh 2008). Recent research has focused on the measurement of guided waves in cortical bone using the axial transmission (AT) configuration (emitter and receiver placed on the same site). Guided waves depend both on the geometry and on the material properties of the propagation medium. Accordingly, an *ex vivo* study revealed that the phase velocity of the A_0 mode (υ_{A0}), measured at 200 kHz, was significantly correlated with cortical thickness (Ct.Th) ($R^2 = 0.52$, $p < 0.001$) and vBMD ($R^2 = 0.45$, $p < 0.001$) (Muller et al. 2005). Furthermore, it is also possible to extract the dispersion curves of multiple guided wave modes (Minonzio et al. 2010) and to predict them analytically using a 2-D transverse isotropic free plate model (Foiret et al. 2014). If constant stiffness of the bone matrix is then assumed, cortical porosity (Ct.Po) and Ct.Th can be obtained from the fitted theoretical dispersion curves (Bochud et al. 2016). Recently, this approach was validated *ex vivo* on 31 radii and 15 tibiae from human cadavers with site-matched micro-CT (Minonzio et al. 2018).

To date, guided wave measurements were performed in our group using a 1-MHz probe optimized for the radius. Recent *ex vivo* (Kroker et al. 2017) and *in vivo* (Sundh et al. 2017) studies suggest that cortical bone parameters measured at the tibia are strong predictors of hip fracture. These findings motivated us to develop a novel AT probe for ultrasound measurements at the tibia that exhibits a larger Ct.Th range (2−6 mm) compared with the radius (1−4 mm) (Karjalainen et al. 2008). To optimize the excitation of guided waves, we decreased the central frequency to 500 kHz and slightly increased the probe dimensions. The novel probe was used previously *ex vivo* on 17 tibiae and could successfully predict Ct.Po ($R^2 = 0.83$, root mean square error [RMSE] = 2.2%) and Ct.Th ($R^2 = 0.57$, RMSE 0.37 mm) measured by site-matched micro-CT (Schneider et al., 2019). The aim of this study was to test the 500-kHz probe for the first time *in vivo* at the tibia in a small group of patients. We compared the results obtained from the ultrasound measurements with those for site-matched pQCT and ultradistal HR-pQCT.

METHODS

Patients

Twenty patients (mean age: 51 ± 14 y, mean body mass index: 25.5 ± 3.0 kg/m^2) participated in this study. The study cohort represented a subgroup of 8 women and 12 men participating in two different ongoing studies. The first study was a population-based cross-sectional study approved by the local ethics committee (EA4/095/05), as well as by the German Radiation Protection Ordinance (Z5-22462/2-2005-063). The second study was a randomized controlled trial, Preventing the Impairment of Primary Osteoarthritis by High Impact Long-Term Physical Exercise Regimen, approved by the local ethics committee (EA4/027/15), as well as by the German Radiation Protection Ordinance (Z5-22462/2-2015-027). Written informed consent was obtained from all participants before recruitment.

Peripheral quantitative computed tomography

The proximal third of the tibia (66% of the lower-limb length up from the lateral malleolus of the fibula) of all patients was imaged using a clinical pQCT scanner (XCT2000, Stratec Medizintechnik GmbH, Pforzheim, Germany) according to our previously described procedure (Rittweger et al. 2000). The voxel size was 0.5 × 0.5 × 2.3 mm. The cortical volumetric bone mineral density ($Ct.vBMD_{pQCT}$) was determined as the average across a single cross-sectional scan using the manufacturer's software package (threshold: 711 mg/cm^3). A custom MATLAB (The MathWorks, Natick, MA, USA) program was used to calculate the cortical thickness ($Ct.Th_{pQCT}$) based on the only available cross-sectional slice (Fig. 1b) downloaded from the scanner per patient. The tibia cross section was cropped manually before the image was binarized using Otsu's (1979) method. Subsequently, $Ct.Th_{pQCT}$ was defined as the minimum distance between the endosteal and periosteal surfaces (Chappard et al. 2013) at the medial portion of the tibia and above the medullary canal, according to the location of the ultrasound measurement.

High-resolution peripheral quantitative computed tomography

The ultradistal tibia (standard protocol, starting at 22.5 mm from the tibial endplate) of 8 patients was imaged using a clinical HR-pQCT scanner (XtremeCT I, Scanco Medical AG, Brüttisellen, Switzerland) according to our previously described procedure (Armbrecht et al. 2011). Each scan consisted of 110 slices with a nominal isotropic resolution of 82 μm. The total volumetric bone mineral density ($Tt.vBMD_{XCT}$) was obtained from the standard morphologic analysis (Boutroy et al. 2005). Then, the cortical bone compartment was segmented according to the morphologic analysis described by Burghardt et al. (2010). The following parameters were calculated based on these cortical bone volumes: $Ct.vBMD_{XCT}$, $Ct.Th_{XCT}$, cortical pore diameter ($Po.Dm_{XCT}$) and cortical porosity ($Ct.Po_{XCT}$). The scripts provided by the manufacturer were used.

Dual-energy X-ray absorptiometry

Dual-energy X-ray absorptiometry (DXA, iDXA, GE Medical Systems, WI, USA, software EnCore v13) was used to measure aBMD at the whole body

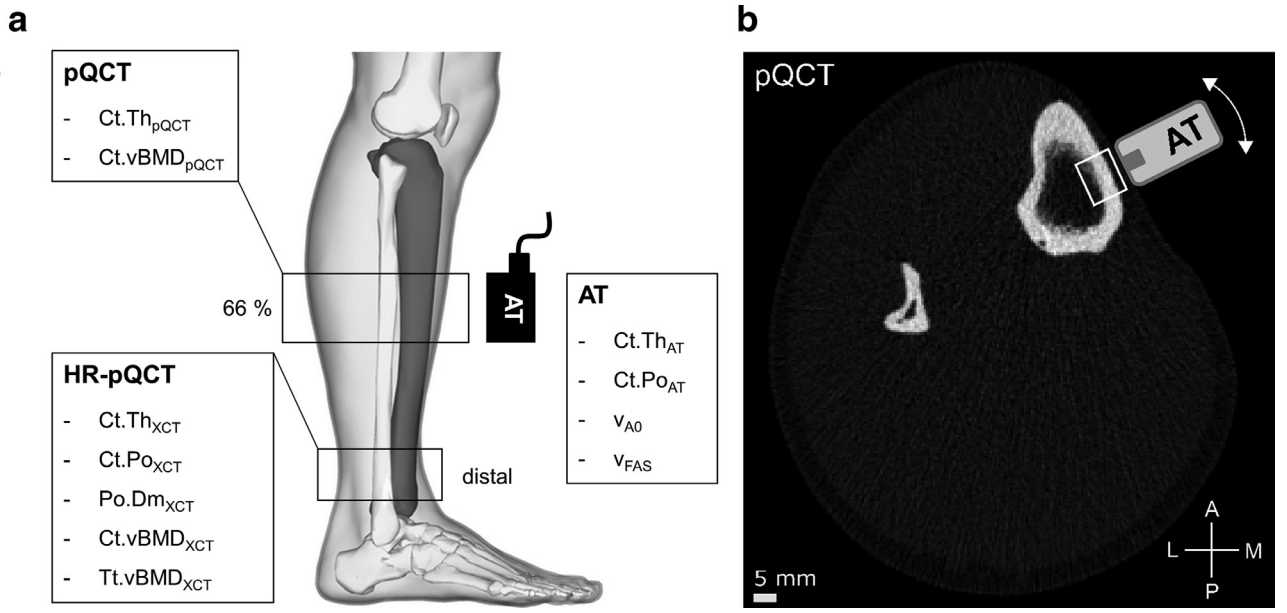

Fig. 1. (a) Overview of measurements. Five hundred-kilohertz axial transmission (AT) was performed site-matched with pQCT (voxel size: 500 μm) at the proximal third of the tibia (66%). The distal site of the same limb was scanned with HR-pQCT (voxel size: 82 μm). (b) Cross-sectional pQCT image illustrating the tangential position of the ultrasound probe, which was slowly tilted in both circumferential directions (*arrow*) during the acquisition of 400 individual measurements. The side view of the lower limb was generated with the BodyParts3D/Anatomography service (DBCLS, Japan). HR-pQCT = high-resolution peripheral quantitative computed tomography.

($aBMD_{WB}$), lumbar spine ($aBMD_{LS}$, L1–L4 in the posterior–anterior projection) and total femur ($aBMD_{TF}$). All scans and analyses were performed by the same operator to ensure consistency and standard quality control procedures. Patients were classified as normal or osteopenic based on their total femur *T*-score in accordance with World Health Organization criteria (Kanis 1994).

Axial transmission

An ultrasound bi-directional AT system (Azalée, Paris, France) consisting of a custom-made probe (Vermon, Tours, France), driving electronics (Althais, Tours, France) and a human machine interface (HMI, Bleu-Solid, Paris, France) was used. The multichannel probe had a central 24-receiver array (pitch = 1.2 mm) and two lateral five-emitter arrays (pitch = 1.5 mm). The dimensions of each rectangular receiver and emitter were 1.2×13 and 1.5×13 mm^2, respectively. A distance of 8 mm separated the receiver array from each emitter array. This configuration enabled the propagation of ultrasound in two opposite directions, a technique that is used to correct errors induced by small inclination angles between the probe and the bone surface (Moreau et al. 2014). A wideband pulse with a center frequency of 500 kHz (−6-dB frequency bandwidth from 0.3 to 0.7 MHz) was used to excite the five multi-element transmitters successively with time delays ranging from 0 to 0.8 μs. One hundred twenty radiofrequency (RF) signals, corresponding to all possible receiver–transmission pairs, were digitized (12 bits, 20 MHz, 1024 samples) for each propagation direction after 16 averages performed by the hardware.

The ultrasound measurements were performed at the proximal third of the tibia (66%) according to the pQCT scan location (Fig. 1a). The probe was placed at the anteromedial surface of the tibia (facies medialis) aligned with the long axis of the bone. Acoustic coupling gel was used to ensure sound transmission to and from the body. The circumferential position of the probe is illustrated in Figure 1b. One measurement cycle consisted of 400 subsequent measurements. The reproducibility was assessed by repeating the acquisition of a cycle at least three times with intermediate probe repositioning. During each cycle the probe was slowly tilted in both circumferential directions to scan a wide region above the medullary cavity. During every measurement 120 RF signals (5×24) were acquired from each propagation direction. The scan time per cycle was about 3 min.

$Ct.Th_{AT}$ and $Ct.Po_{AT}$ were estimated by fitting a 2-D transverse isotropic free plate model to the measured dispersion curves as described in detail elsewhere (Minonzio et al. 2018). Briefly, the recorded time signals were transformed to the frequency–wavenumber (f–k) space using a 2-D spatiotemporal Fourier transform

enhanced with singular value decomposition. This provided the so-called *Norm function,* of which each pixel (*f, k*) reflected the presence rate of a wave mode on a 0 to 1 scale (Minonzio et al. 2010). Then, a database of dispersion curves from a 2-D transverse isotropic free plate model was projected onto the singular vector basis to obtain the objective function (Minonzio et al. 2018). The dispersion curves of the plate model were generated from a set of effective stiffness tensors which were predicted for different thickness−porosity combinations (Bochud et al. 2016; Parnell et al. 2012). We thereby assumed that the transverse isotropic elastic coefficients (c_{11} = 26.8 GPa, c_{13} = 15.3 GPa, c_{33} = 35.1 GPa and c_{55} = 7. 3 GPa) and mass density (ρ = 1.91 g/cm^3) for the tissue matrix are invariant (Granke et al. 2011).

The objective function of the projection was obtained and optimized to find the best fit between the theoretical and experimental dispersion curves (Fig. 2a). Often, we obtained more than one local maximum mainly because of incomplete experimental dispersion curves. Such model ambiguities were removed by comparing the two highest local maxima for each of the 400 measurements of a cycle. When the highest local maximum exceeded the secondary maximum of at least 10%, this was considered to be a valid solution to the problem. Otherwise, the single measurement was rejected. If at least 10 of the 400 measurements produced a valid parameter pair, the medians of Ct.Po/Ct.Th were calculated. Otherwise, the entire measurement cycle was rejected. Finally, if at least two cycles were valid, the medians of the corresponding cycles were averaged for every specimen. Otherwise, the entire measurement series for that sample was rejected.

The velocity of the first arriving signal (υ_{FAS}) was calculated based on a bi-directional measurement principle (Bossy et al. 2004). Briefly, the time of flight was determined for each emitter−receiver distance using the first extremum of the signal in the time domain. The sound velocity was then derived from the inverse slope of a linear fit through the measured times of flight plotted versus the known emitter−receiver distances. This procedure was performed for each of the five emissions and from both directions to account for small inclination angles between the probe and the bone surface. Unstable measurements for which the absolute difference between two opposite velocities was larger than 50 m/s (Talmant et al. 2009) were eliminated. Ideally, a single measurement provided five corrected velocities, which were then averaged. Velocity histograms were obtained for each cycle, and υ_{FAS} was calculated as the average of the histogram peaks.

The A_0 mode phase velocity (υ_{A0}) was calculated in the frequency range 0.4 to 0.5 MHz (Fig. 2b). First, the Norm function was expressed in the frequency-phase velocity domain ($c_{phase} = 2\pi f/k$) (Minonzio et al. 2010). Then, its amplitudes were averaged over frequency in the phase velocity c_{phase} range 1400 to 1900 m/s, and υ_{A0} was defined as the maximum position of the averaged Norm function. The harmonic mean of the velocities from the two opposite emissions was calculated to correct for inclination angles between the probe and the bone surface (Bossy et al. 2004). Similarly to υ_{FAS},

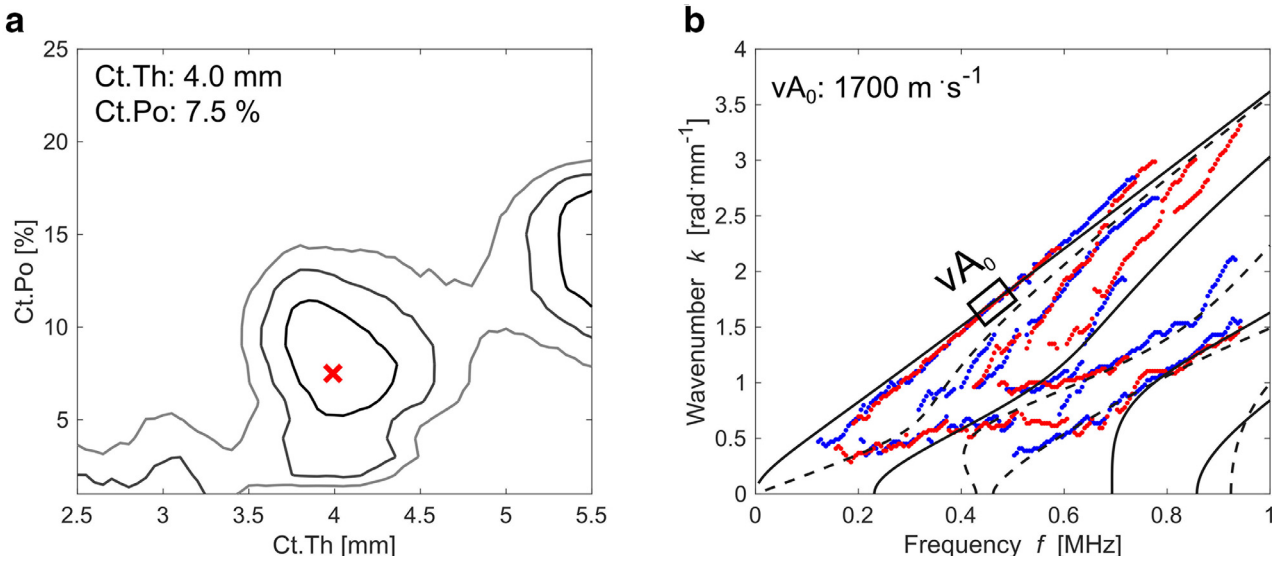

Fig. 2. (a) Contour plot depiction of the objective function. The *red cross* indicates the global maximum, corresponding to the best fit (b) between the transverse isotropic free plate model (*continuous and dashed lines*) and the measured dispersion curves (*red and blue dots*). The red and blue colors of the dots correspond to the two opposite directions of the bi-directional guided wave measurements.

measurements for which the absolute difference between two opposite velocities was larger than 50 m/s were considered unstable and eliminated. The subject's final υ_{A0} was calculated by averaging the peak values of the velocity histograms obtained for each cycle.

Statistical analysis

Linear regression analysis and Pearson's correlation coefficients were used to quantify the degree of association between site-matched parameters obtained with AT and pQCT. Associations between AT and HR-pQCT were assessed using Spearman's rank-correlation coefficient. AT (N = 15), pQCT (N = 15) and HR-pQCT (N = 8) parameters were normally distributed as determined by Shapiro–Wilk tests. The Bland–Altman plot was used to reveal biases in the prediction of $Ct.Th_{pQCT}$. Differences between the means were tested with paired *t*-tests. Correlations were considered statistically significant for p values < 0.05. The AT *in vivo* single-cycle repeatability ($Ct.Th_{AT}$, $Ct.Po_{AT}$, υ_{FAS} and υ_{A0}) was estimated using the root-mean-square average of the standard deviation of repeated cycles for each measured patient (Glüer et al. 1995). Unless stated otherwise, all image processing and statistical analysis were performed using MATLAB (R2017a).

RESULTS

The ultrasound measurements from 15 of 20 patients were used for statistical analysis. Five patients were excluded after evaluating the pQCT scans because $Ct.Th_{pQCT}$ was below 2.5 mm. In such thin cortical layers, our ultrasound transducer does not excite sufficient guided wave modes (in particular those existing at higher frequencies) because of its limited frequency bandwidth. Thirteen of the 15 patients received DXA scans at the proximal femur. The total femur *T*-score was used to classify the patients into two groups: osteopenic ($-2.5 < T\text{-score} < -1.0$, N = 4) and normal ($T\text{-score} > -1.0$, N = 9). Note that no osteoporotic patients ($T\text{-score} < -2.5$) were included. Between both groups, no statistically significant differences were found for the AT, pQCT and HR-pQCT parameters. The single-cycle repeatability of the ultrasound measurements was 0.13 mm for $Ct.Th_{AT}$, 1.6% for $Ct.Po_{AT}$, 25.8 m/s for υ_{FAS} and 17.2 m/s for υ_{A0}. The measurement data obtained in the study sample are summarized in Table 1.

The R^2 values of the linear regression between AT and site-matched pQCT parameters are listed in Table 2. $Ct.vBMD_{pQCT}$ was best correlated with $Ct.Po_{AT}$ ($R^2 = 0.57$, $p < 0.001$, Fig. 3a) followed by υ_{FAS} ($R^2 = 0.43$, $p < 0.01$) and υ_{A0} ($R^2 = 0.28$, $p < 0.05$). Good agreement was found between $Ct.Th_{AT}$ and $Ct.Th_{pQCT}$ ($R^2 = 0.62$, $p < 0.001$, RMSE = 0.39). When one outlier was excluded, the correlation improved significantly ($R^2 = 0.90$, $p < 0.001$, RMSE = 0.19, Fig. 3b) and decreased the mean difference between both methods from 0.39 to 0.23 mm in the Bland–Altman plot (Fig. 3c). There was a statistically significant difference between the values of both methods with ($p = 0.013$) and without ($p = 0.009$) the outlier.

We compared the AT parameters with those of distal HR-pQCT and found a strong correlation between υ_{FAS} and $Tt.vBMD_{XCT}$ (Spearman's $\rho = 0.98$, $p = 0.0004$, Fig. 4). The negative correlation between $Ct.Po_{AT}$ and $Tt.vBMD_{XCT}$ was the second strongest but did not reach the significance level (Spearman's $\rho = -0.64$, $p = 0.096$).

Table 1. Descriptive statistics

	Mean ± SD	Range	N
Axial transmission			
$Ct.Th_{AT}$ (mm)	4.0 ± 0.7	3.1–5.1	15
$Ct.Po_{AT}$ (%)	12.7 ± 4.2	5.3–20	15
υ_{A0} (m/s)	1626 ± 67	1491–1711	15
υ_{FAS} (m/s)	3918 ± 40	3838–3965	15
pQCT			
$Ct.vBMD_{pQCT}$ (mg/cm^3)	1176 ± 26	1134–1208	15
$Ct.Th_{pQCT}$ (mm)	3.7 ± 0.8	2.7–5.1	15
HR-pQCT			
$Ct.Th_{XCT}$ (mm)	1.3 ± 0.4	0.7–1.7	8
$Ct.Po_{XCT}$ (%)	5.5 ± 1.6	2.8–7.5	8
$Po.Dm_{XCT}$ (μm)	123 ± 11	102–136	8
$Ct.vBMD_{XCT}$ (mg/cm^3)	842 ± 56	769–928	8
$Tt.vBMD_{XCT}$ (mg/cm^3)	296 ± 77	176–381	8
DXA			
$aBMD_{LS}$ (mg/cm^2)	1.19 ± 0.16	0.98–1.50	13
$aBMD_{TF}$ (mg/cm^2)	1.04 ± 0.19	0.76–1.29	13
$aBMD_{WB}$ (mg/cm^2)	1.32 ± 0.14	1.07–1.50	15

DXA = dual-energy X-ray absorptiometry; HR-pQCT = high-resolution peripheral quantitative computed tomography; SD = standard deviation.

Table 2. R^2 of the linear regression between parameters from site-matched axial transmission and peripheral quantitative computed tomography (N = 15)

	$Ct.Th_{pQCT}$	$Ct.vBMD_{pQCT}$
$Ct.Th_{AT}$	0.62§	ns
$Ct.Po_{AT}$	ns	(−) 0.57§
υ_{A0}	0.31†	0.28†
υ_{FAS}	ns	0.43‡

ns = not significant.
*The associations are positive unless otherwise indicated by a negative sign.
† $p < 0.05$.
‡ $p < 0.01$.
§ $p < 0.001$.

We compared the AT parameters with those of distal HR-pQCT and found a strong correlation between υ_{FAS} and $Tt.vBMD_{XCT}$ (Spearman's $\rho = 0.98$, $p = 0.0004$, Fig. 4). The negative correlation between $Ct.Po_{AT}$ and $Tt.vBMD_{XCT}$ was the second strongest but did not reach the significance level (Spearman's $\rho = -0.64$, $p = 0.096$).

DISCUSSION

In this *in vivo* pilot study, we used a novel 500-kHz tibia probe to measure guided waves successfully in 15

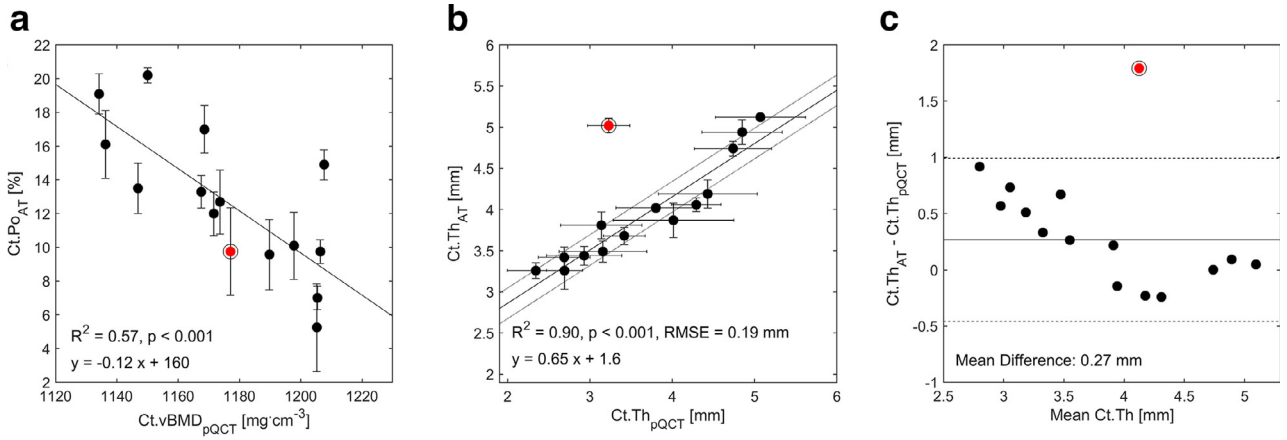

Fig. 3. Axial transmission versus site-matched peripheral quantitative computed tomography parameters measured at the proximal third of the tibia (N = 15). Linear regressions between (a) $Ct.Po_{AT}$ and $Ct.vBMD_{pQCT}$ and (b) $Ct.Th_{AT}$ and $Ct.Th_{pQCT}$ after exclusion of red outlier marked with circle. The correlation including the outlier was $R^2 = 0.62$, $p < 0.001$, root mean square error = 0.39 mm. The *dotted lines* in (b) indicate the root mean square error. (c) Bland–Altman plot of $Ct.Th_{AT}$ and $Ct.Th_{pQCT}$. Mean difference and lines were calculated without outlier. Mean difference with outlier was 0.33 mm. *Dashed lines* indicate 95% confidence intervals at ± 1.96 standard deviation.

patients. Excellent agreement was obtained between $Ct.Th_{AT}$ and site-matched $Ct.Th_{pQCT}$ when one outlier was removed. Moreover, $Ct.Po_{AT}$ correlated moderately with site-matched $Ct.vBMD_{pQCT}$. We adapted the ultrasound signal processing from a previously reported *ex vivo* study using a 1-MHz AT probe designed for measurements at the radius (Minonzio et al. 2018). In that way, $Ct.Th_{AT}$ and $Ct.Po_{AT}$ were obtained automatically from a 2-D transverse isotropic free plate model, which was fitted to the extracted dispersion curves. We also modified the former *in vivo* measurement protocol (Vallet et al. 2016): The number of measurements per cycle was increased from 10 to 400, and the probe was slowly tilted in both circumferential directions during the acquisitions, instead of performing static measurements. Thus, we maintained a similar single cycle repeatability *in vivo* (Ct.Po: 1.6%, Ct.Th: 0.13 mm) as previously reported *ex vivo* using the 1-MHz probe (Ct.Po = 1.9%, Ct.Th = 0.11 mm) (Minonzio et al. 2018).

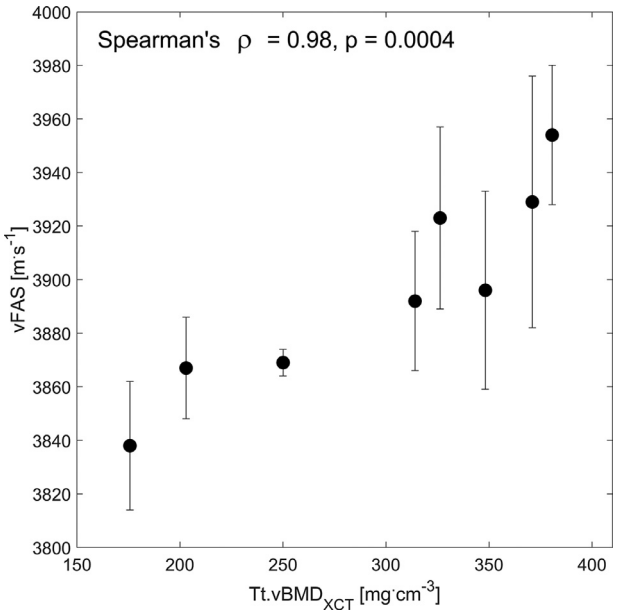

Fig. 4. Correlation between υ_{FAS} at the midshaft and distal $Tt.vBMD_{XCT}$ with strong Spearman's rank-correlation coefficient ($\rho = 0.98$, $p < 0.001$, N = 8). Vertical error bars represent standard deviations (within at least three repeated cycles).

A moderate correlation between site-matched $Ct.Po_{AT}$ and $Ct.vBMD_{pQCT}$ was found ($R^2 = 0.57$, $p < 0.001$). Because vBMD is a strong predictor of Ct.Po ($R = -0.88$, $p < 0.001$) (Ostertag et al. 2016), a stronger correlation could have been expected. Several factors could have contributed to it. First, the AT and pQCT scan regions were not exactly site-matched. The pQCT device scanned only a 2.3-mm-thick section, whereas the region scanned by AT was much larger (*i.e.,* approximately 29 mm, according to the length of the receiver array). Second, $Ct.vBMD_{pQCT}$ was calculated from the entire cortical compartment, whereas AT scanned only the facies medialis (Fig. 1b). A more precise $Ct.vBMD_{pQCT}$ evaluation, that is, smaller region of interest, would have caused unreliable estimates because of the limited number of available cortical bone voxels (pQCT is a single-slice method with in-plane spatial resolution of 0.5 mm). In a recent *ex vivo* study using the same probe and site-matched μCT (with a 39-μm isotropic voxel size), we found a stronger correlation between $Ct.Po_{AT}$ and $Ct.vBMD_{\mu CT}$ ($R^2 = 0.80$, $p < 0.001$) (Schneider et al., under revision). To achieve this, we had the means to adequately segment the cortical

compartment (Burghardt et al. 2010) and considered only the volume below the receiver array. Moreover, these e*x vivo* measurements were conducted without overlaying soft tissue, which might have improved the correlation.

It is possible that soft tissue negatively affected the quality of our signals, reducing the accuracy of the fit between the plate model and the experimental dispersion curves. The accurate estimation of waveguide properties was previously reported despite the presence of soft tissue modes, but only in 4 patients and using a 1-MHz AT probe (Bochud et al. 2017). In that study, a bilayer model was proposed to account for additional soft tissue modes. However, the authors finally suggested using the plate model, because it was able to predict the experimental modes of the cortical waveguide equally well as the bilayer model, but with less complexity and computational cost. On the basis of this finding, we used the simpler plate model to predict the dispersion curves measured in this study at the tibia.

Five of 20 patients had to be excluded because they had thin cortical bone layers at the ultrasound measurement site ($Ct.Th_{pQCT} < 2.5$ mm). Interestingly, 3 of these 5 excluded cases were significantly older (73 ± 6 y) than the mean age of the 15 patients analyzed (47 ± 10 y). The decreased Ct.Th of these elderly patients might have been caused by endosteal trabecularization, which their pQCT scans also indicated. However, the two other excluded patients were relatively young (35 and 43 y), indicating that thin cortical bone at the tibia is present in patients of different ages. As a solution, the 1-MHz probe, originally designed for measurements at the thinner radius, could be used at the tibia when guided waves are not sufficiently excited using the 500-kHz probe. In the future, capacitive micromachined ultrasonic transducers (CMUTs) might allow the design of a probe with a larger frequency bandwidth. CMUTs in combination with a smaller pitch, although keeping a similar receiver array length, could significantly enhance the detection of guided wave modes over a larger Ct.Th range.

It is a limitation that the distal tibiae of only 8 patients were scanned with HR-pQCT. Thus, the linear regression analysis between the AT and distal HR-pQCT measurement parameters needs to be considered with caution because of the small sample size. However, we found a statistically significant correlation (υ_{FAS} vs. $Tt.vBMD_{XCT}$, Fig. 4) that underlines the sensitivity of this parameter to systemic microstructural changes. This finding suggests that guided wave measurements conducted at the midshaft tibia may also reflect microstructural changes at relevant fracture sites, such as the proximal femur. However, tibial υ_{FAS} at 250 kHz has previously been found to correlate only weakly with femoral strength (Bouxsein et al. 1999) and to be a poor discriminant of osteoporotic fracture (Stegman et al. 1995). To date, only one study investigated the direct association between Ct.Po at the tibia midshaft and femoral neck fracture strength ($R = -0.50$, $p < 0.001$, $N = 56$) (Abraham et al. 2015). A strength of our ultrasound system is that it measures four cortical bone parameters at the same time ($Ct.Th_{AT}$, $Ct.Po_{AT}$, υ_{FAS} and υ_{A0}), which may provide improved fracture prediction combined using multivariate models. The scope of forthcoming studies will be to relate these four ultrasound parameters to hip fracture, alone or in conjunction with other measurements.

In this study, we used a first-generation HR-pQCT system (XCT-I, isotropic voxel size: 82 μm), which allows scanning of only the distal tibia (Boyd 2008). At this site, we could not conduct site-matched guided wave measurements because the cortex is too thin ($Ct.Th < 2$ mm) and the facies medialis is not flat enough. We did not find any statistically significant correlation between the AT and cortical HR-pQCT parameters ($Ct.Th_{XCT}$, $Ct.Po_{XCT}$, $Po.Dm_{XCT}$, $Ct.vBMD_{XCT}$). Only υ_{FAS} against $Tt.vBMD_{XCT}$ reached the significance level (Fig. 4). However, this correlation needs to be considered with caution because of the small sample size. One reason for the absence of significant correlations between the cortical AT and HR-pQCT parameters may be the distinct characteristic pattern of trabecular and cortical bone mass distributions across the tibia. For example, toward the epiphyses, cortical bone exhibits significantly lower vBMD values compared with more proximal sites (Kamer et al. 2016). Furthermore, little cortical bone is present at the standard HR-pQCT ultradistal measurement site. Therefore, cortical parameters should be assessed more proximally (Ostertag et al. 2014; Sundh et al. 2017). This is possible with the second-generation HR-pQCT (XCT-II, isotropic voxel size: 61 μm), which allows scanning of the tibia midshaft at even higher resolution (Ensrud et al. 2018). Consequently, future guided wave studies should be conducted with the site-matched XCT-II to improve the accuracy of reference thickness estimates. Moreover, it would be of great interest to observe the correlation between $Ct.Po_{AT}$ and site-matched $Ct.Po_{XCT}$, although the HR-pQCT scanner cannot accurately measure small pores with diameters less than 100 μm (Cooper et al. 2016; Ostertag et al. 2014, 2016).

We found a moderate correlation between υ_{FAS} and $Ct.vBMD_{pQCT}$ ($R^2 = 0.43$, $p < 0.01$, Table 1). This finding is in agreement with previously reported *in vivo* measurements of tibial υ_{FAS} at different frequencies: 200 kHz (Moilanen et al. 2003), 400 kHz (Kilappa et al. 2010) and 1.25 MHz (Sievänen et al. 2001). We did not find a statistically significant correlation between υ_{FAS} and $Ct.Th_{pQCT}$ similarly to the studies at 400 kHz

(Kilappa et al. 2010) and 1.25 MHz (Sievänen et al. 2001). Only the study at 200 kHz (Moilanen et al. 2003) found a weak but statistically significant correlation ($R = 0.24$, $p < 0.05$), indicating that larger wavelengths, reaching deeper into the cortex, are needed to obtain a dependency between υ_{FAS} and Ct.Th at the tibia (Bossy et al. 2005). The reproducibility of υ_{FAS} (0.7 %) obtained in this study is in line with other *in vivo* studies, as, for example, the 1.8% obtained by Moilanen et al. (2003).

Compared with that of υ_{FAS}, the measurement of υ_{A0} has been less studied *in vivo*. Here, we found that υ_{A0} correlated moderately with $Ct.Th_{pQCT}$ and $Ct.vBMD_{pQCT}$. This was expected because the velocities of guided waves depend on both thickness and material properties, that is, represented here by $Ct.vBMD_{pQCT}$. Furthermore, these results agree with a clinical study using 200-kHz AT at the tibia of pubertal girls to measure υ_{A0} (Moilanen et al. 2003). However, in that study the wave packages of the A_0 mode were extracted in the time domain, whereas we isolated the A_0 dispersion in the frequency-phase velocity domain. The authors report that 22% of their υ_{A0} measurements were judged unreliable because of interference with soft tissue, in which ultrasound propagates at velocities (~1500 m/s) similar to those of the A_0 mode in cortical bone (Moilanen et al. 2008). In our study, we observed a regular disappearance of the A_0 mode at higher frequencies (0.5−1.0 MHz), particularly in patients with thick soft tissue layers. Thus, to improve robustness, we chose to estimate υ_{A0} in a lower and narrower frequency range (0.4−0.5 MHz, Fig. 2b) compared with what we used *ex vivo* (0.5−0.8 MHz) (Schneider et al. 2019). Consequently, we did not observe any υ_{A0} failure case and our *in vivo* reproducibility (1.1%) was superior to that of Moilanen et al. (2008), 2.3%.

CONCLUSIONS

It is possible to estimate Ct.Po and Ct.Th at the tibia using a novel 500-kHz AT probe. Good agreement was found between $Ct.Th_{AT}$ and site-matched $Ct.Th_{pQCT}$. We found a moderate correlation between $Ct.Po_{AT}$ and site-matched $Ct.vBMD_{pQCT}$ which was used as a surrogate for Ct.Po. The second-generation HR-pQCT (XCT-II), which allows measurements at the tibia midshaft with significantly enhanced resolution compared with pQCT, is now on the market. Further *in vivo* studies should be conducted site-matched with XCT-II to improve the accuracy of reference estimates. The measurement of guided waves at the tibia might improve the prediction of bone fractures in a cost-effective and radiation-free manner.

Acknowledgments—Funding for this work was provided by the Deutsche Forschungsgemeinschaft (DFG) through the Berlin−Brandenburg School for Regenerative Therapies GSC 203 and Project TacoSound (Ra1380/9-1) and by the Bundesministerium für Bildung und Forschung (BMBF, musculoskeletal research network OVERLOAD-PrevOP [Subproject SPP6] and Subproject 01EC1408L "characterization of cortical and subchondral bone"). We thank Ahmed BenSaïda for the MATLAB implementation of the Shapiro−Wilk test and Gianluca Iori for his cortical thickness calculation algorithm.

REFERENCES

Abraham AC, Agarwalla A, Yadavalli A, McAndrew C, Liu JY, Tang SY. Multiscale predictors of femoral neck in situ strength in aging women: Contributions of BMD, cortical porosity, reference point indentation, and nonenzymatic glycation. J Bone Miner Res 2015;30:2207–2214.

Armbrecht G, Belavý DL, Backström M, Beller G, Alexandre C, Rizzoli R, Felsenberg D. Trabecular and cortical bone density and architecture in women after 60 days of bed rest using high-resolution pQCT: WISE 2005. J Bone Miner Res Off J Am Soc Bone Miner Res 2011;26:2399–2410.

Bochud N, Vallet Q, Bala Y, Follet H, Minonzio JG, Laugier P. Genetic algorithms-based inversion of multimode guided waves for cortical bone characterization. Phys Med Biol 2016;61:6953.

Bochud N, Vallet Q, Minonzio JG, Laugier P. Predicting bone strength with ultrasonic guided waves. Sci Rep 2017;7:43628.

Bossy E, Talmant M, Laugier P. Bi-directional axial transmission improves accuracy and precision of ultrasonic velocity measurement in cortical bone. IEEE Trans Ultrason Ferroelectr Freq Control 2004;51:71–79.

Bossy E, Padilla F, Peyrin F, Laugier P. Three-dimensional simulation of ultrasound propagation through trabecular bone structures measured by synchrotron microtomography. Phys Med Biol 2005;50:5545.

Boutroy S, Bouxsein ML, Munoz F, Delmas PD. In Vivo Assessment of Trabecular Bone Microarchitecture by High-Resolution Peripheral Quantitative Computed Tomography. J Clin Endocrinol Metab 2005;90:6508–6515.

Bouxsein ML, Coan BS, Lee SC. Prediction of the strength of the elderly proximal femur by bone mineral density and quantitative ultrasound measurements of the heel and tibia. Bone 1999;25:49–54.

Boyd SK. Site-specific variation of bone micro-architecture in the distal radius and tibia. J Clin Densitom 2008;11:424–430.

Burghardt AJ, Buie HR, Laib A, Majumdar S, Boyd SK. Reproducibility of direct quantitative measures of cortical bone microarchitecture of the distal radius and tibia by HR-pQCT. Bone 2010;47:519–528.

Chappard C, Bensalah S, Olivier C, Gouttenoire PJ, Marchadier A, Benhamou C, Peyrin F. 3D characterization of pores in the cortical bone of human femur in the elderly at different locations as determined by synchrotron micro-computed tomography images. Osteoporos Int 2013;24:1023–1033.

Cooper DML, Kawalilak CE, Harrison K, Johnston BD, Johnston JD. Cortical bone porosity: What is it, why is it important, and how can we detect it? Curr Osteoporos Rep 2016;14:187–198.

Ensrud KE, Vo TN, Burghardt AJ, Schousboe JT, Cauley JA, Taylor BC, Hoffman AR, Orwoll ES, Lane NE, Langsetmo L. for the Osteoporotic Fractures in Men (MrOS) Research Group. Weight loss in men in late life and bone strength and microarchitecture: A prospective study. Osteoporos Int 2018;29:1549–1558.

Foiret J, Minonzio JG, Chappard C, Talmant M, Laugier P. Combined estimation of thickness and velocities using ultrasound guided waves: A pioneering study on *in vitro* cortical bone samples. IEEE Trans Ultrason Ferroelectr Freq Control 2014;61:1478–1488.

Glüer DCC, Blake G, Lu Y, Blunt1 BA, Jergas1 M, Genant1 HK. Accurate assessment of precision errors: How to measure the reproducibility of bone densitometry techniques. Osteoporos Int 1995;5:262–270.

Granke M, Grimal Q, Saïed A, Nauleau P, Peyrin F, Laugier P. Change in porosity is the major determinant of the variation of cortical bone elasticity at the millimeter scale in aged women. Bone 2011;49:1020–1026.

Kamer L, Noser H, Blauth M, Lenz M, Windolf M, Popp AW. Bone mass distribution of the distal tibia in normal, osteopenic, and osteoporotic conditions: An ex vivo assessment using HR-pQCT,

DXA, and computational modelling. Calcif Tissue Int 2016;99: 588–597.
Kanis JA. Assessment of fracture risk and its application to screening for postmenopausal osteoporosis: Synopsis of a WHO report. WHO Study Group. Osteoporos Int 1994;4:368–381.
Karjalainen J, Riekkinen O, Töyräs J, Kröger H, Jurvelin J. Ultrasonic assessment of cortical bone thickness *in vitro* and *in vivo*. IEEE Trans Ultrason Ferroelectr Freq Control 2008;55:2191–2197.
Kilappa V, Moilanen P, Xu L, Nicholson PHF, Timonen J, Cheng S. Low-frequency axial ultrasound velocity correlates with bone mineral density and cortical thickness in the radius and tibia in pre- and postmenopausal women. Osteoporos Int 2010;22:1103–1113.
Kroker A, Plett R, Nishiyama KK, McErlain DD, Sandino C, Boyd SK. Distal skeletal tibia assessed by HR-pQCT is highly correlated with femoral and lumbar vertebra failure loads. J Biomech 2017;59: 43–49.
Langton CM, Njeh CF. The measurement of broadband ultrasonic attenuation in cancellous bone—A review of the science and technology. IEEE Trans Ultrason Ferroelectr Freq Control 2008;55:1546–1554.
Lespessailles E, Hambli R, Ferrari S. Osteoporosis drug effects on cortical and trabecular bone microstructure: A review of HR-pQCT analyses. BoneKEy Rep 2016;5 836.
Minonzio JG, Talmant M, Laugier P. Guided wave phase velocity measurement using multi-emitter and multi-receiver arrays in the axial transmission configuration. J Acoust Soc Am 2010;127:2913–2919.
Minonzio JG, Bochud N, Vallet Q, Bala Y, Ramiandrisoa D, Follet H, Mitton D, Laugier P. Bone cortical thickness and porosity assessment using ultrasound guided waves: An *ex vivo* validation study. Bone 2018;116:111–119.
Moilanen P, Nicholson PHF, Kärkkäinen T, Wang Q, Timonen J, Cheng S. Assessment of the tibia using ultrasonic guided waves in pubertal girls. Osteoporos Int 2003;14:1020–1027.
Moilanen P, Talmant M, Kilappa V, Nicholson P, Cheng S, Timonen J, Laugier P. Modeling the impact of soft tissue on axial transmission measurements of ultrasonic guided waves in human radius. J Acoust Soc Am 2008;124:2364–2373.
Moreau L, Minonzio JG, Talmant M, Laugier P. Measuring the wavenumber of guided modes in waveguides with linearly varying thickness. J Acoust Soc Am 2014;135:2614–2624.
Muller M, Moilanen P, Bossy E, Nicholson P, Kilappa V, Timonen J, Talmant M, Cheng S, Laugier P. Comparison of three ultrasonic axial transmission methods for bone assessment. Ultrasound Med Biol 2005;31:633–642.
Neto GPC, Pereira RMR, Alvarenga JC, Takayama L, Funari MFA, Martin RM. Evaluation of bone mineral density and microarchitectural parameters by DXA and HR-pQCT in 37 children and adults with X-linked hypophosphatemic rickets. Osteoporos Int 2017; 28:1685–1692.
Ostertag A, Peyrin F, Fernandez S, Laredo JD, de Vernejoul MC, Chappard C. Cortical measurements of the tibia from high resolution peripheral quantitative computed tomography images: A comparison with synchrotron radiation micro-computed tomography. Bone 2014;63:7–14.
Ostertag A, Peyrin F, Gouttenoire PJ, Laredo JD, DeVernejoul MC, Solal MC, Chappard C. Multiscale and multimodality computed tomography for cortical bone analysis. Phys Med Biol 2016; 61:8553.
Otsu N. A threshold selection method from gray-level histograms. IEEE Trans Syst Man Cybern 1979;9:62–66.
Parnell WJ, Vu MB, Grimal Q, Naili S. Analytical methods to determine the effective mesoscopic and macroscopic elastic properties of cortical bone. Biomech Model Mechanobiol 2012;11:883–901.
Rittweger J, Beller G, Ehrig J, Jung C, Koch U, Ramolla J, Schmidt F, Newitt D, Majumdar S, Schiessl H, Felsenberg D. Bone-muscle strength indices for the human lower leg. Bone 2000;27:319–326.
Schneider J, Iori G, Ramiandrisoa D, Hammami M, Gräsel M, Chappard C, Barkmann R, Laugier P, Grimal Q, Raum K. Ex vivo cortical porosity and thickness predictions at the tibia using full spectrum ultrasonic guided wave analysis. Arch Osteoporos (2019) 14: 21. https://doi.org/10.1007/s11657-019-0578-1.
Schuit SCE, van der Klift M, Weel AEAM, de Laet CEDH, Burger H, Seeman E, Hofman A, Uitterlinden AG, van Leeuwen JPTM, Pols HAP. Fracture incidence and association with bone mineral density in elderly men and women: The Rotterdam Study. Bone 2004;34:195–202.
Sievänen H, Cheng S, Ollikainen S, Uusi-Rasi K. Ultrasound velocity and cortical bone characteristics in vivo. Osteoporos Int 2001;12:399–405.
Stegman MR, Heaney RP, Travers-Gustafson D, Leist J. Cortical ultrasound velocity as an indicator of bone status. Osteoporos Int 1995;5:349–353.
Sundh D, Nilsson AG, Nilsson M, Johansson L, Mellström D, Lorentzon M. Increased cortical porosity in women with hip fracture. J Intern Med 2017;281:496–506.
Talmant M, Kolta S, Roux C, Haguenauer D, Vedel I, Cassou B, Bossy E, Laugier P. In vivo performance evaluation of bi-directional ultrasonic axial transmission for cortical bone assessment. Ultrasound Med Biol 2009;35:912–919.
Vallet Q, Bochud N, Chappard C, Laugier P, Minonzio JG. In vivo characterization of cortical bone using guided waves measured by axial transmission. IEEE Trans Ultrason Ferroelectr Freq Control 2016;63:1361–1371.
Wainwright SA, Marshall LM, Ensrud KE, Cauley JA, Black DM, Hillier TA, Hochberg MC, Vogt MT, Orwoll ES. Hip fracture in women without osteoporosis. J Clin Endocrinol Metab 2005;90: 2787–2793.